Sensing atmospheric turbulence by GNSS phase observations

Markus Vennebusch, Steffen Schön

Institut für Erdmessung, Leibniz Universität Hannover, Germany, eMail: vennebusch@ife.uni-hannover.de

Atmospheric turbulence

Signals of Global Navigation Satellite Systems (GNSS), as well as all other electromagnetic waves are effected by atmospheric attenuation, scintillation, and delay. Especially the dry (hydrostatic) and wet (non-hydrostatic) signal delays are one of the main error sources which have to be adequately accounted for when using GNSS signals for e.g. precise surveying or timing purposes. These tropospheric delays show both long periodic and short periodic variations in the range from months to hours as well as from minutes to seconds (and even less). The short periodic behaviour is caused by high-frequency variations of the refractivity index *n* which are generated by turbulent air motions within the first approximately 2000 [m] of the atmosphere (i.e., the atmospheric boundary layer).

Temporal stochastic behaviour of tropospheric delays

Atmospheric turbulence is characterised as a non-stationary stochastic process. Consequently it should not be expressed in terms of (auto-)correlation functions or power spectral densities. A more appropriate tool to assess the temporal behaviour of a non-stationary process *X* is the temporal structure function (Wheelon 2001)

$$D_X(\tau) = \langle [X(t+\tau) - X(t)]^2 \rangle \tag{1}$$

with < > denoting an ensemble average and τ indicating the time lag between two values of *X*. The temporal differencing removes data trends and thus generates a difference process which is usually stationary even if the original time series is not stationary.

An explicit expression for the temporal structure function of phase measurements (and tropospheric delays) is provided by (Wheelon 2001) as follows (see Tab. 1):

$$D_\varphi(\tau) = D_T(\tau) = 1.564 R k^2 C_n^2 k_0^{-\frac{5}{3}} \times \left(1 - \frac{2^{\frac{1}{6}}}{\Gamma\left(\frac{5}{6}\right)} (\kappa_0 v \tau)^{\frac{5}{6}} K_{\frac{5}{6}}(\kappa_0 v \tau)\right) \tag{2}$$

Figure 1 shows the explicit temporal structure function, Eq. (2), for various typical turbulence parameter sets evaluated for a fixed observation geometry with an elevation of 13.5 [°].

For all parameter combinations considered, the explicit temporal structure functions show a clear 5/3 power-law behaviour for the first ~80 [s]. Depending on the specified turbulence parameters (especially the outer scale length L_0) a continous decrease of the exponent can be seen. At a maximum of approximately 500 [s] the exponent reaches zero (for these examples), i.e., the time series can be considered to be uncorrelated.

Figure 1: Explicit temporal structure functions of slant tropospheric delays for typical conditions of atmospheric turbulence for a fixed observation geometry with an elevation of 13.5 [°].

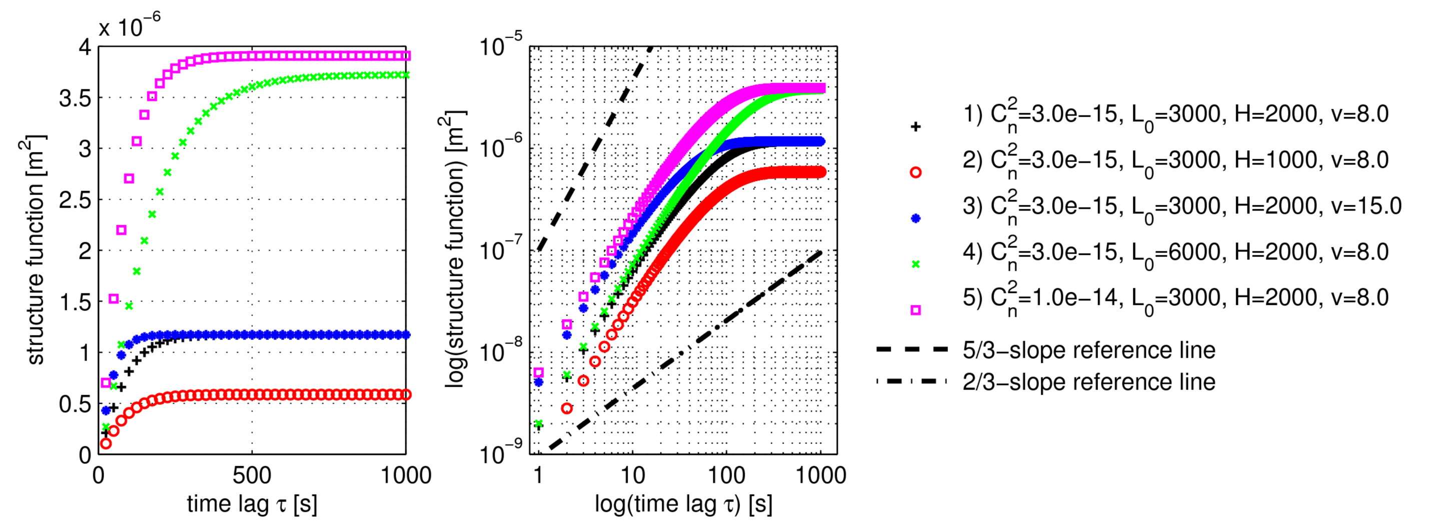

Covariance expression of slant tropospheric delays

Variances and covariances of tropospheric delays can be derived by integrating the spectrum of refractivity variations along the lines-of-sight (Wheelon 2001). A general covariance expression for tropospheric delays has been derived by Schön and Brunner (2008). Based on the von Karman spectrum and the assumptions of height-independent C_n^2, local isotropy, uniform wind speed and wind direction this formulation describes the covariance of two tropospheric slant delays $T_A^i(t_A)$ and $T_B^j(t_B)$ at two stations A and B, to two satellites i and j and at two epochs t_A and t_B. In its most general formulation the co-variance expression reads:

$$\langle T_A^i(t_A), T_B^j(t_B) \rangle = \frac{12}{5} \frac{0.033}{\Gamma\left(\frac{5}{6}\right)} \frac{\sqrt{\pi^3} \kappa_0^{-\frac{2}{3}} 2^{-\frac{1}{3}}}{\sin \varepsilon_A^i \sin \varepsilon_B^j} C_n^2 \times \int_0^H \int_0^H (\kappa_0 d)^{\frac{1}{3}} K_{-\frac{1}{3}}(\kappa_0 d) \, dz_1 \, dz_2 \tag{3}$$

Simulation of slant tropospheric delay variations

Using real or simulated observation geometries as well as adequate turbulence parameters a fully occupied variance-covariance matrix Σ_T of tropospheric delays *T* can be set up to generate simulated tropospheric delay variations. In the following, these variations will be simulated by using an orthonormal matrix *G* containing the eigenvectors of Σ_T, a diagonal matrix Λ containing the square roots of the eigenvalues of Σ_T on its main diagonal, and a vector *x* of gaussian random numbers with zero mean and unit variance via:

$$\boldsymbol{y} = \boldsymbol{G}\sqrt{\boldsymbol{\Lambda}}\boldsymbol{x} \tag{4}$$

For the simulation of slant tropospheric delay variations a realistic geometry of a rising GPS satellite is used. During an observation period of 1000 [s] (~17 [min]) the satellite rises from 10 [°] to 17 [°] elevation at an azimuth of 201 [°]. Using a sampling rate of 0.1 [Hz] the entire observation period yields 100 observations.

Parameter set 1 (Average turbulence conditions): The simulated slant tropospheric delay variations vary in the range of +/- 2 [mm] with an average variance of 4.6 x 10^{-7} [m²]. All temporal structure functions show a clear 5/3 power-law behaviour for the first 180-200 [s].

Parameter set 2 (Wind azimuth increased): Changing the wind azimuth α_v from 0 [°] to 90 [°] has a significant decorrelating effect on the simulated tropospheric delays. The slant delay time series show much rougher behaviour which obviously agrees with the reduced correlation lengths. The slopes of the temporal structure functions are generally smaller than 5/3, especially for small time lags τ. This behaviour results from the increased roughness (reduced correlation) of the simulated time series yielding an apparent high-frequency noise contribution. The impact of wind on the (co-)variances can be explained by analysing the separation distance *d* (see Eq. (3)).

Parameter set 3 (Wind speed increased): Increasing the wind speed *v* from 8 [m/s] to 15 [m/s] also has a decorrelating effect on tropospheric delay variations. This can also be observed in larger values of the temporal structure functions. Again, no exact 5/3 power-law behaviour can be observed for small time lags τ.

In summary, the general behaviour (e.g., the 5/3 slope and the variations due to parameter changes) of the structure functions of simulated tropospheric delays agrees with the general behaviour of the explicit temporal structure functions. However, especially for small time lags τ discrepancies of a factor of almost five are observed. This needs to be further investigated.

Stochastic behaviour of slant tropospheric delays derived from 'Precise Point Positioning' (PPP)

In addition to simulated slant delays, we investigated zenith tropospheric delays derived from PPP solutions. Figure 6 (top) shows that estimated ZTD time series for each station of a specially designed network (see Fig. 5) show very similar behaviour with hourly variations of approximately +/- 1 [cm]. The bottom plot shows the temporal structure functions of each station's ZTD time series with a clear 5/3 power-law behaviour of the first approximately 300 [s]. After a transition phase (for time lags of approximately 300 to 1000 [s]) with a 2/3 power-law behaviour the slope finally approaches zero (indicating uncorrelated ZTDs).

References

Schön S, Brunner FK: Atmospheric turbulence theory applied to GPS carrier-phase data, J geod 82(1): 47-57, 2008.
Wheelon AD: Electromagnetic scintillation-I. Geometrical optics, Cambridge University Press, Cambridge, 2001.

Acknowledgements

The authors thank the German Research Foundation (Deutsche Forschungsgemeinschaft) for its financial support (SCHO 1314/1-1).

Variable:	Description:	Variable:	Description:
C_n^2	Structure constant of refractivity	α_v	Wind direction (azimuth)
$k_0 = 2\pi/L_0$	Wave number to corresponding outer scale length L_0	ε_v	Wind direction (elevation)
a=b=c	Elongations of turbulent structures (a, b: horizontal, c: vertical)	H	Height of wet troposphere (integration height)
e_A^i	Elevation of satellite i at station A	d	separation distance between the actual integration points
v_0	Wind velocity		

Table 1: Parameter descriptions.

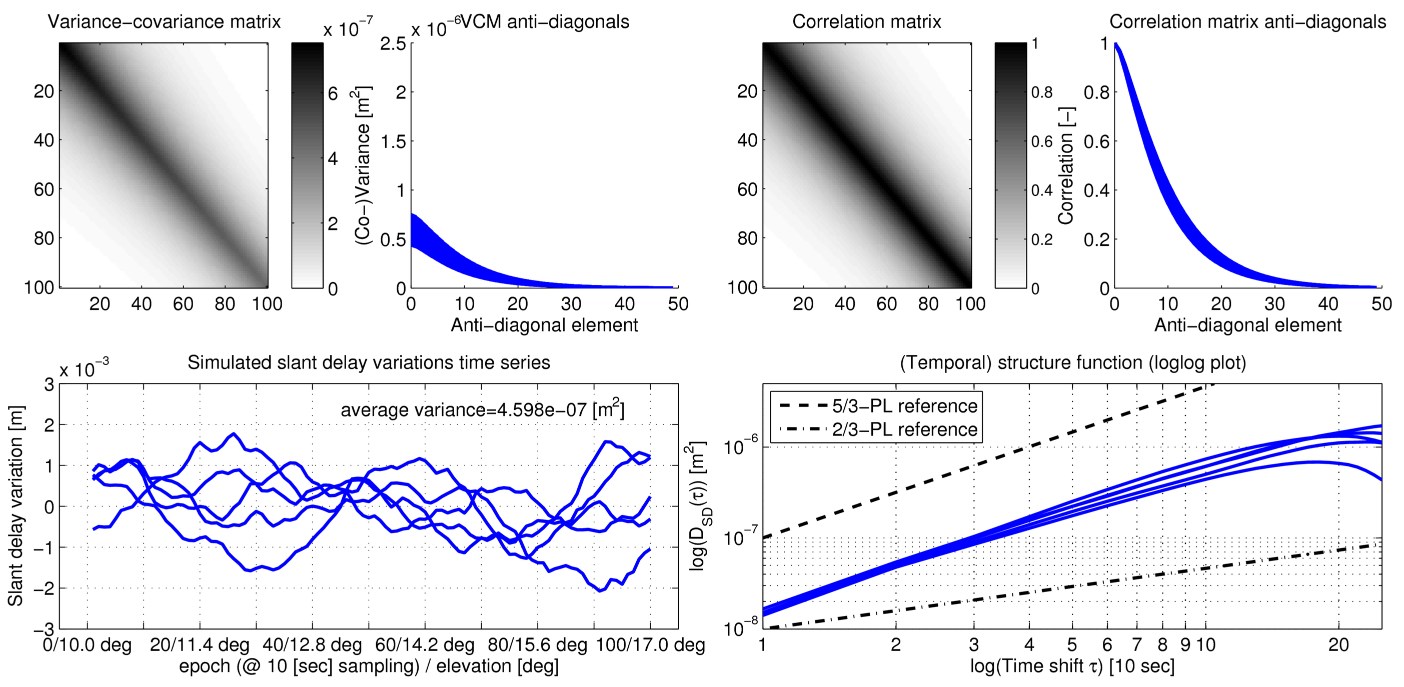

Figure 2: Variance-covariance matrix, correlation matrix, anti-diagonals, simulated slant tropospheric delay variations and their temporal structure functions for average turbulence parameters (C_n^2 = 0.3 x 10^{-14} [$m^{-2/3}$], outer scale length L_0=3000 [m], integration height H=2000 [m], wind speed v=8 [m/s] and wind direction α_v=0 [°]).

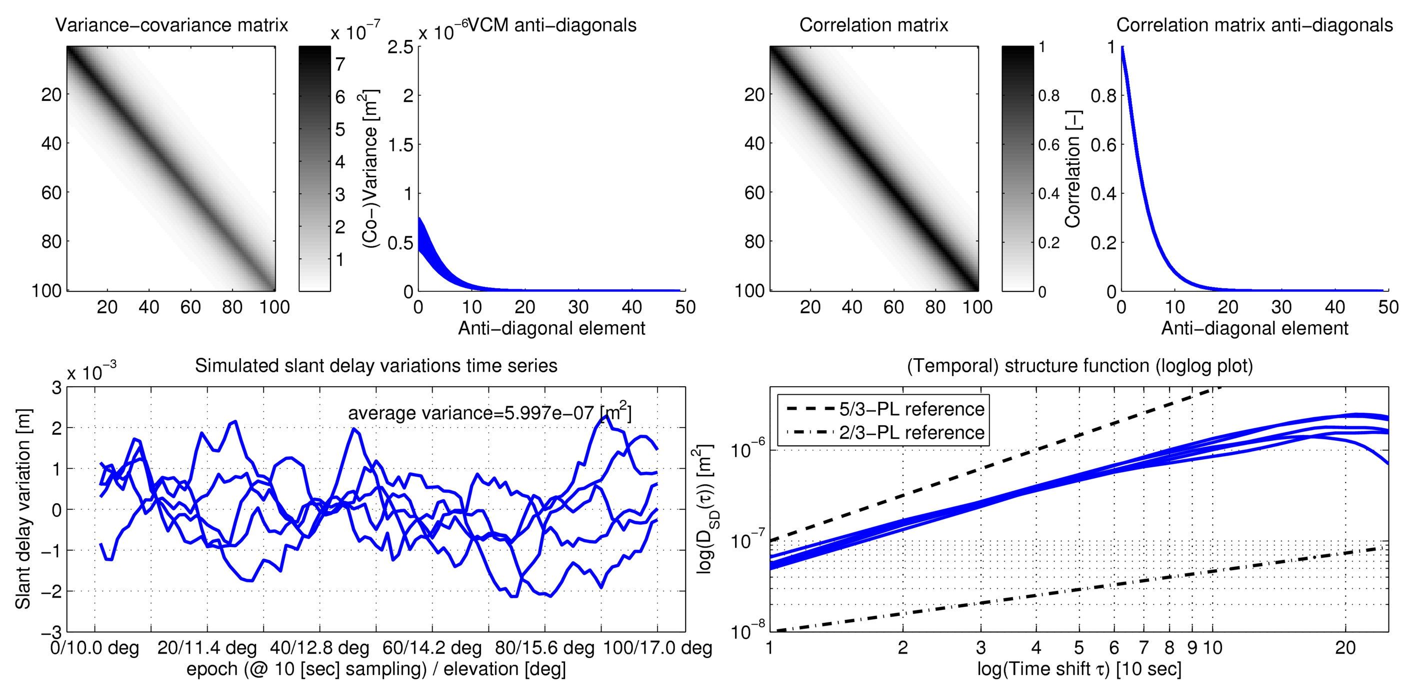

Figure 3: Same as Fig. 2, but wind azimuth increased (C_n^2 = 0.3 x 10^{-14} [$m^{-2/3}$], outer scale length L_0=3000 [m], integration height H=2000 [m], wind speed v=8 [m/s], wind direction α_v=90 [°]).

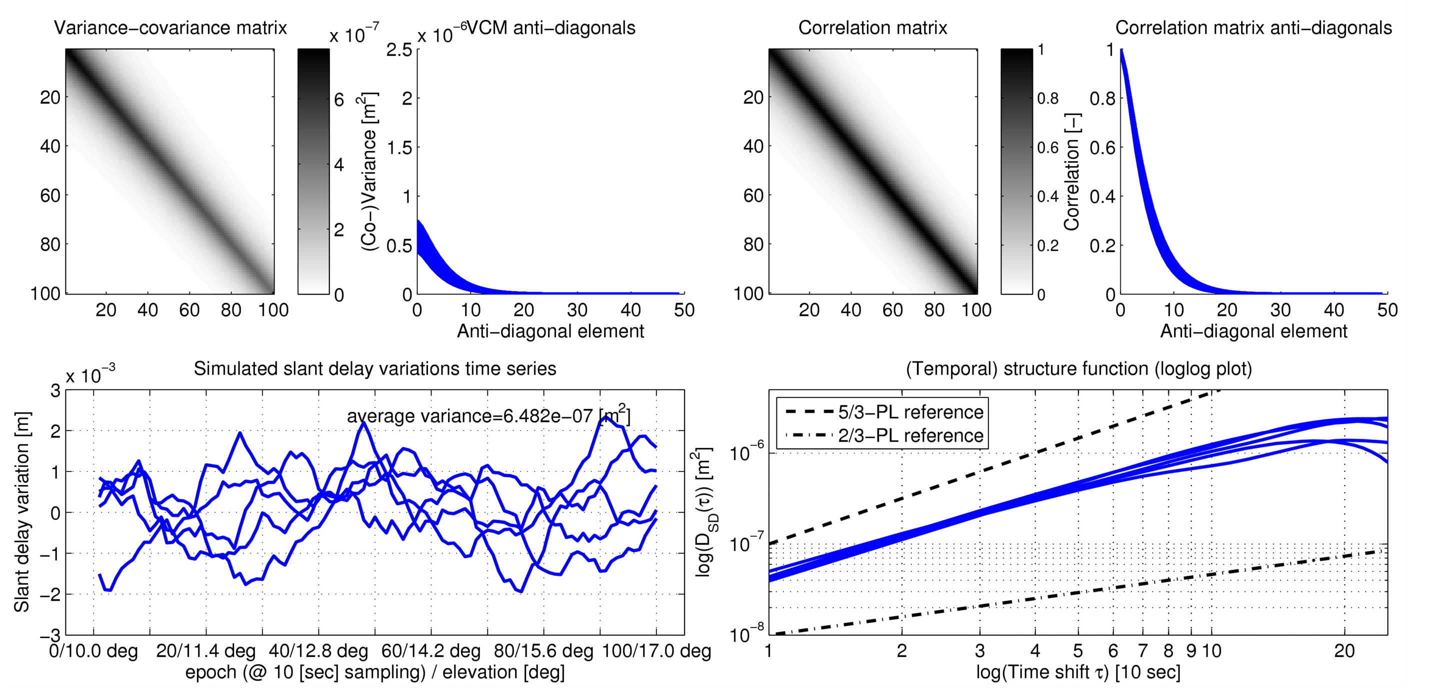

Figure 4: Same as Fig. 2, but wind speed increased (C_n^2 = 0.3 x 10^{-14} [$m^{-2/3}$], outer scale length L_0=3000 [m], integration height H=2000 [m], wind speed v=15 [m/s], wind direction α_v=0 [°]).

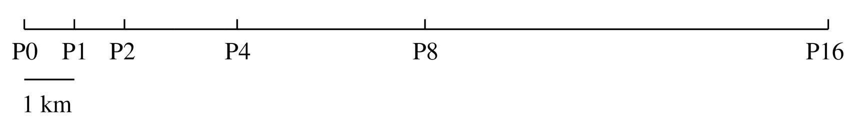

Figure 5: Geometry of 'Seewinkel GPS network' (Austria).

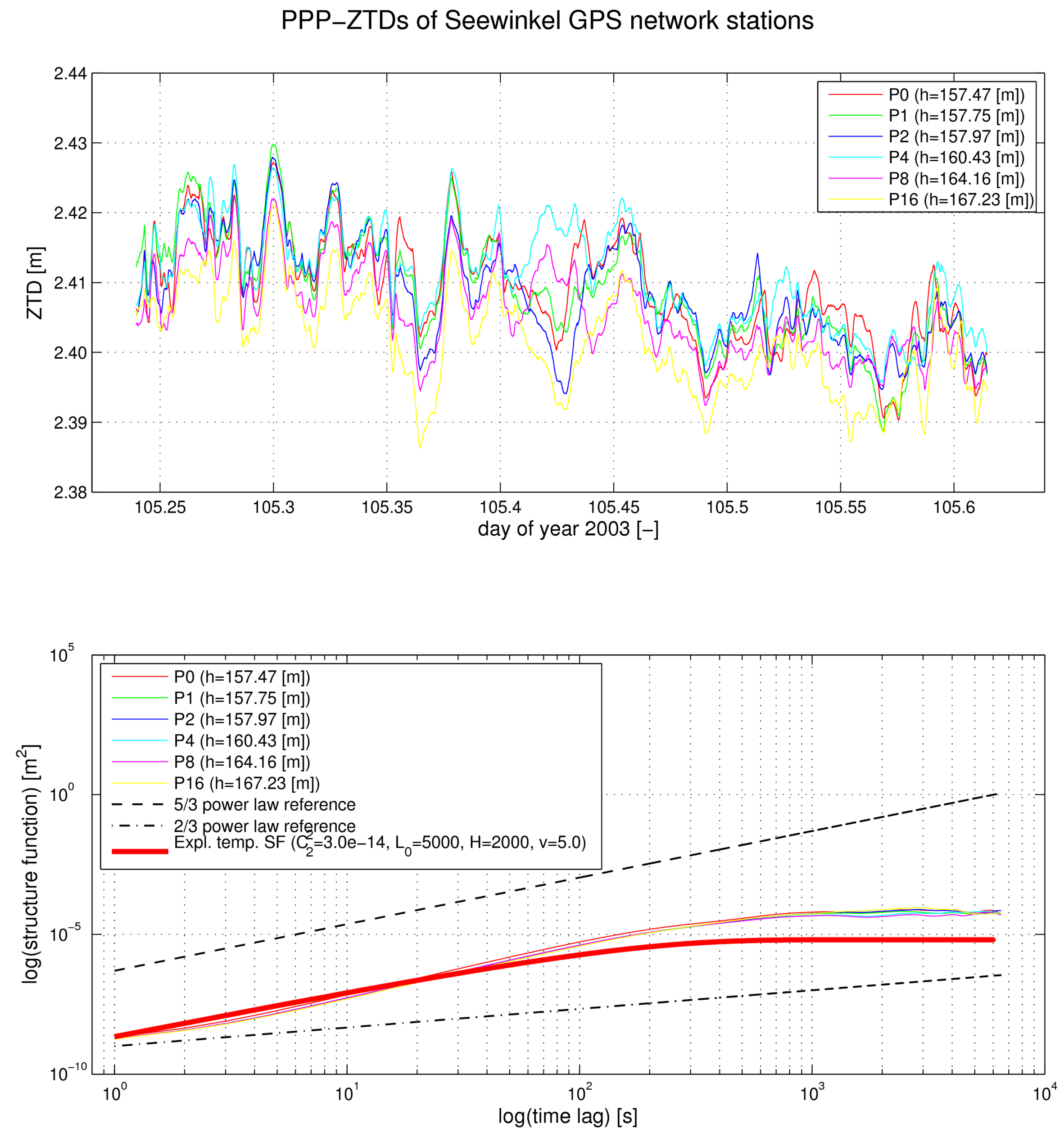

Figure 6: Zenith tropospheric delays obtained by a 'Precise Point Positioning' solution of GNSS code and phase observations (top). Temporal structure functions of zenith tropospheric delays (bottom).